Atomic structure of metallic interfaces

1996 J. Phys. D: Appl. Phys. 29 1689

(http://iopscience.iop.org/0022-3727/29/7/003)

J. Phys. D: Appl. Phys. **29** (1996) 1689–1698. Printed in the UK

Atomic structure of metallic interfaces

A T Paxton†

Department of Materials, Parks Road, Oxford OX1 3PH
SRI International, Menlo Park, CA94025, USA

Received 14 August 1995

Abstract. The atomic structure of the (310) symmetric tilt grain boundary in Nb and of an interface between Mo and Re is calculated. The calculations are done within the tight binding (TB) approximation to quantum mechanics and are checked carefully against some accurate first-principles calculations in the local density approximation to density functional theory. A non-orthogonal spd electron TB model is tested, but is found to be no improvement on the much simpler orthogonal d-electron model; in particular there is no improvement in the volume dependence of the total energy. The structure of the Nb grain boundary is compared to that obtained by other authors using high resolution electron microscopy. The comparison enables some statements to be made about the nature of the interatomic interactions and especially about the opposing forces that are balanced at the equilibrium grain boundary expansion. The paper includes the first quantum mechanical calculation of a dissimilar metal interface with a view to obtaining the structure of a misfit dislocation and a value for the theoretical strength of the interface. It is concluded that the misfit dislocation in this case has a widely spread core and that the theoretical strength is considerably reduced relative to the bulk crystal.

1. Introduction

We would like to use certain prescriptions for the interatomic forces to calculate the atomic structure of interfaces. If this turns out to be a reliable calculation then we could learn something about the nature of the bonding at interfaces, defects, electronic structure and so on. Since at present the only prescription known to be wholly reliable, namely the local density functional theory, is also very difficult and costly to use it is important to make rigorous comparisons of the more approximate calculations with experimental measurements. Over the last decade or so it has been popular practice to compare calculated atomic structures with those measured by high-resolution electron microscopy (HREM); nowadays with the use of a first principles quantum mechanical approach one can make comparisons with experimentally obtained absorption and emission spectra. In the present paper, the former more traditional comparison will be made since, although the calculations will be quantum mechanical, they will for the most part be empirical and hence unable to predict electronic transitions. This paper is divided into two parts. In the first the subject is a grain boundary in Nb; the second is concerned with a dissimilar metal interface in the Mo–Re system. Most calculations are made using the tight-binding (TB) approximation. For the remainder of this introduction the quantum mechanical method for atomistic simulation will be described.

1.1. Density functional theory (DFT)

It is widely accepted that the atomic structure of solids, as well as the electronic structure of all but the highly correlated systems, is very accurately predicted using *density functional theory* in the *local density approximation*. This is not the place to give any details—the reader is referred to a recent book for descriptions of DFT and the tight-binding approximation to be discussed below [1].

Very briefly, in density functional theory, the (negative) cohesive energy of an assembly of atoms in the quantum mechanical ground state is

$$E_B[\rho] = \sum_{i,occ} \varepsilon_i - \frac{1}{2}\int \mathrm{d}\boldsymbol{r}\, \phi_{es}\rho(\boldsymbol{r}) - \int \mathrm{d}\boldsymbol{r}\, \mu_{xc}\rho(\boldsymbol{r}) + E_{xc} + E_{ii} - E_{atoms}. \quad (1)$$

The first term is the intuitively reasonable sum over the energies of the occupied states. Because these are independent electron states, the total energy is corrected by the next three terms (sometimes called 'double counting correction') in which ρ is the electron density, and ϕ_{es} is the classical electrostatic potential associated with the density through Poisson's equation:

$$\nabla^2\phi_{es} = 4\pi e^2\rho. \quad (2)$$

E_{xc} is the exchange and correlation energy which accounts for all the non-classical (many-body) corrections; μ_{xc} is the associated exchange and correlation potential:

$$\mu_{xc} = \frac{\delta E_{xc}[\rho]}{\delta\rho}. \quad (3)$$

† Present address: Department of Pure and Applied Physics, Queen's University, Belfast BT7 1NN, Northern Ireland.

0022-3727/96/071689+10$19.50

E_{ii} is the electrostatic pair repulsion between the nuclei and E_{atoms} is the total energy of the free atoms in vacuo.

In density functional theory, ε_i and ψ_i are eigenvalues and eigenvectors of an effective, single particle Hamiltonian

$$\hat{H} = -\frac{\hbar^2}{2m}\nabla^2 + v_{eff}(\boldsymbol{r})$$

and the Schrödinger equation,

$$\hat{H}\psi_i = \varepsilon_i \psi_i$$

has to be solved self-consistently with the Poisson equation (2) since the 'effective potential'

$$v_{eff} = \phi_{es} + \mu_{xc} + v_{en}$$

depends on the charge density through equation (2). v_{en} is the electrostatic potential due to the positive nuclei.

The only approximation that needs to be made apart from those involving technical details (basis set, Brillouin zone integration and so on) is the local density approximation (LDA) [1]. In density functional theory all the many-body aspects of the problem appear in the quantities E_{xc} and μ_{xc} which are related through the functional derivative in equation (3). It is known that the exchange and correlation energy is a functional of the charge density but the form of the functional is not known. In the local density approximation it is taken to be given at each point in space $\boldsymbol{r}$ by the exchange and correlation energy of a uniform electron gas having the same density $\rho(\boldsymbol{r})$ that is encountered locally at that point. The local density approximation is expressed as

$$E_{xc}^{LDA} = \int \varepsilon_{xc}(\rho)\rho(\boldsymbol{r})\,\mathrm{d}\boldsymbol{r}$$

where $\varepsilon_{xc}(\rho)$ is the exchange and correlation energy density of a uniform electron gas of density ρ. This function is known and can be found in the form of interpolation formulae [2]. The density functional calculations to be described here are made using a method known as full-potential LMTO [3]. We can take it that these calculations represent the best possible solution to Schrödinger's equation that can currently be made.

1.2. Tight-binding approximation

In tight-binding theory the cohesive energy usually takes the general form

$$\tilde{E}_B = \sum_{i,occ} \tilde{\varepsilon}_i + \tilde{E}_{rep} - C \qquad (4)$$

where $\tilde{\varepsilon}$ are the eigenvalues of a parameterized tight-binding Hamiltonian, and $\tilde{E}_{rep} - C$ is supposed to represent the rest of the terms in equation (1) with the constant C fixing the zero of energy with respect to the free atoms. $\tilde{E}_{rep}$ has the form of a pair potential. Foulkes and Haydock [4] and Sutton *et al* [5] were able to justify this form rigorously using the Harris approximation to the self-consistency procedure. In the approach of Sutton *et al*, the repulsive energy represents the changes in electrostatic and exchange-correlation energies in going from free atoms to the solid state and could be shown to a very good approximation to be a pair-wise repulsive energy.

In problems of dissimilar interfaces, it has been argued [6] that a completely non-self-consistent approach may be inappropriate. We therefore sometimes use a self-consistent tight-binding scheme [7, 8]. We want the Hamiltonian to be able to respond to changes in the potential at least in its diagonal matrix elements. This is done in the following way. After solving the Schrödinger equation for the tight-binding Hamiltonian there will be accumulations of charge Δq_k on each atom k at position $\boldsymbol{r}_k$. This will give rise to an approximate electrostatic potential

$$\tilde{\phi}_j = \sum_{k(\neq j)} \frac{e^2}{|\boldsymbol{r}_k - \boldsymbol{r}_j|}\Delta q_k + U\Delta q_j$$

on atom j. This is a sum of two terms [7]: the first is the inter-atomic, Madelung potential assuming the charge on each atom behaves as a point charge; the second is the intra-atomic potential, has opposite sign, and represents the energy penalty of heaping charge onto an atom. The two terms may both be large but tend mostly to cancel each other [7, 8]. The parameter U is supposed to represent an intra-atomic Coulomb integral [7]. $\tilde{\phi}_j$ is then the electrostatic potential at atomic site j seen by an electron described by the tight-binding Hamiltonian. We then adjust the diagonal elements of the Hamiltonian by adding the $\tilde{\phi}_j$ at each site and solve the Schrödinger equation again to obtain a new electrostatic potential. This procedure continues until self-consistency. In this way, the off-diagonal matrix elements remain fixed by their values determined by the parameterization, while the diagonal matrix elements are determined self-consistently. At self-consistency, the electrostatic energy (which must be included in the right-binding energy) is

$$\tilde{E}_{es} = \frac{1}{2}\sum_j \tilde{\phi}_j \Delta q_j.$$

Because of the large cancellation between terms, this is usually so small as to be negligible, as pointed out by Harrison [7]. However, to be strictly correct it must be subtracted from the eigenvalue sum in equation (4) to avoid double counting the electron–electron interaction as in density functional theory. The constant C in equation (4) is the input number of electrons of each angular momentum ℓ on site j, $N_{j\ell}$, times the input diagonal Hamiltonian matrix element $\varepsilon^0_{j\ell}$. Equation (4) becomes

$$\tilde{E}_B = \sum_{i,occ} \tilde{\varepsilon}_i - \tilde{E}_{es} - \sum_{j\ell} N_{j\ell}\varepsilon^0_{j\ell} + \tilde{E}_{rep}.$$

It is not difficult to differentiate at least the first and last terms in this expression to obtain interatomic forces. We will not go into this here but refer the reader to [9] and [10] where details can be found. We have to assume that the charge transfer does not contribute significantly to the force. It is identically zero in the local charge neutrality approximation of Sutton *et al* [5] which amounts to setting $U = \infty$. In fact our approach is to calculate atomic

relaxations without self-consistency and to determine the charge transfer and total energy in a subsequent calculation. This procedure can be iterated to obtain a final fully self-consistent and relaxed structure.

1.3. Parameterization of the TB Hamiltonian

The simplest TB model for a transition metal involves only the d-electrons. It is well known that the attractive contribution to the cohesion comes from localized directional bonds between d-states, and that the s-band provides a uniform positive pressure [11, 12]. This can be seen in figure 1. The s-pressure cannot be reproduced in a simple TB model even if overlap (non-orthogonality) is included since the largest contribution to the pressure comes from overlap between the free-electron like s-electrons and atomic core states. We have constructed d-band tight-binding models for Mo, Re and Nb and a non-orthogonal spd model also for Nb. The models are based on original parameterizations by Spanjaard and Desjonquères [14]. The two-centre matrix element of the Hamiltonian (and overlap) connecting two atoms separated by a distance r takes the form

$$h(r) = -f\mathrm{e}^{-qr}$$

and a pair potential of the form

$$\varphi(r) = b\mathrm{e}^{-pr}$$

is used. For the d-band models the values of p and q given by Spanjaard and Desjonquères are used for Mo and Re; we have adjusted p in Nb to obtain a positive value of the c_{44} elastic constant. Given p and q, there are only two free parameters for each metal, namely the prefactors f and b. The latter are adjusted to obtain the correct lattice constant (atomic volume) and f is chosen to obtain the same width of the d-band as found in a self-consistent band calculation.

If the model includes only d-electrons in the Hamiltonian, the number of d-electrons N_d is a parameter, not necessarily the number of d-electrons in the free atom. In that case, the cohesive energy in equation (4) is not strictly with respect to free atoms but to some vacuum reference state in which the number of d-electrons is N_d. The most sensible choice of N_d should be guided by exact band calculations. A difficulty in obtaining the correct structures for Mo and Re arises from the startling fact that in Mo the bcc structure is strongly favoured, while in Re, conversely, the bcc structure is very unfavourable. This is shown in figure 2 which shows hcp–fcc and bcc–fcc energy differences calculated using band theory. It is well known that what determines the stability of transition metals is simply the number of d electrons. However, the rapid rise in the bcc–fcc energy difference with a change in N_d of less than one cannot be reproduced in a simple TB model. We have tried adjusting N_d and found that the best value for Mo is the band theory value of 4.39; but if we choose the 5.12 appropriate for Re, then the bcc structure is stabilized, so that to guarantee the correct ordering of crystal structures we have to set $N_d^{Re} = 6$. For the Nb d-band model $N_d^{Nb} = 3.67$ is used; in the spd model the system contains exactly five electrons and

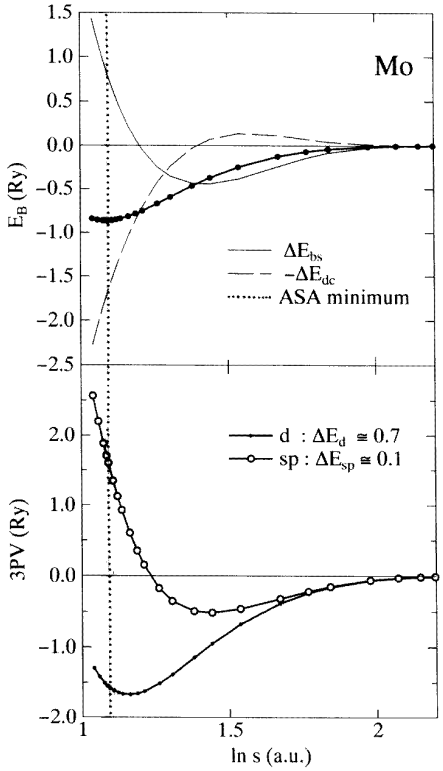

Figure 1. These are band theory calculations of the contributions to the cohesive energy (top panel) and pressure (lower panel) as non-spin polarized Mo atoms are brought from infinity in the vacuum together to form the bcc crystal. The equilibrium volume is indicated by the vertical dotted line; and there we see that the cohesion is a balance of a band contribution ΔE_{bs}, which is the first term in equation (1) and renormalization contribution $-\Delta E_{dc}$ which represents the other terms in equation (1). In the lower panel, we see clearly that the d-electron contribution to the pressure is negative (attractive) and the contribution from the free-electron like sp-electrons is positive. As noted in the text, this latter effect cannot be reproduced in a simple TB band theory and is relegated to the repulsive pair-potential. The atomic volume is represented as the logarithm of the Wigner–Seitz radius s in this plot: the contributions to the cohesive energy from sp- and d-electrons separate out simply as the areas under the curves from equilibrium to infinite volume. For further discussion, see [11–13].

N_d is not a disposable parameter. Figure 3 shows a comparison of the band structure and density of states in Nb for the d-band and spd-band models compared with a local density approximation bandstructure. Note that the value of $N_d^{Nb} = 3.67$ has been chosen to put the Fermi level into agreement with the LDA. This is important in reproducing the softness of the c_{44} elastic constant. In the spd model the Fermi levels fall naturally into the right place and N_d comes out to be 4.14 (this does not happen properly if the p-band is excluded—in that case the total number of electrons would again have to be treated as a disposable parameter, less than five). It is important to include the p-electrons if this is to happen. Parameters of the d-band models are shown in table 1. The values of U for Mo and Re are taken from band theory calculations

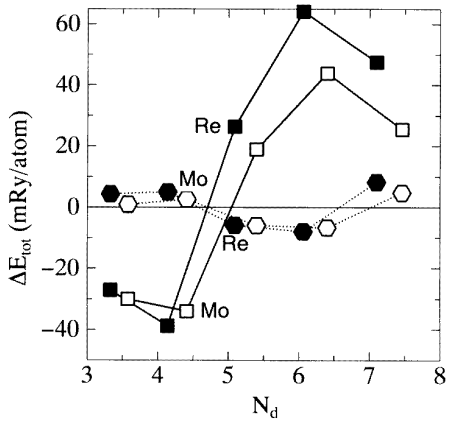

Figure 2. Energy differences between the bcc and fcc lattices (squares) and hcp and fcc lattices (hexagons) in the 4d (open symbols) and 5d (closed symbols) central transition metals (groups 5–9) [16]. Both the energies and d-electron numbers are determined from band theory. Note the rapid destabilization of the bcc phase over a very small change in N_d. This effect cannot be reproduced in a simple d-band TB model.

Table 1. Parameters of the d-band tight-binding models for Nb, Mo and Re. All numbers are in atomic Rydberg units.

	p	*q*	*f*	*b*	N_d	*U*
Mo	1.9513	0.6621	0.4679	1408.8	4.39	0.85
Re	2.0316	0.6687	0.5900	1893.9	6.00	0.87
Nb	1.7790	0.5220	0.2600	747.7	3.67	

[15].

The parameters of the spd model for Nb are as follows (in atomic Rydberg units: 1 Ry = 13.6 eV; 1 Bohr = 0.529 Å). For the Hamiltonian, $\varepsilon_s^0 - \varepsilon_d^0 = 0.2$, $\varepsilon_p^0 - \varepsilon_d^0 = 0.45$, $f_{ss} = -1.5$, $f_{sp} = 1$, $f_{pp} = 2$, $f_{sd} = -0.8$, $f_{pd} = -1$, $f_{dd} = 0.24$. For the overlap, $f_{ss} = 1$, $f_{sp} = -2$, $f_{pp} = -0.2$, $f_{sd} = 1.6$, $f_{pd} = f_{dd} = 0$. For both of these, $q_{ss} = q_{sp} = q_{pp} = q_{sd} = 0.56$, $q_{dd} = 0.522$. For the pair potential, $p = 1.4809$ and $b = 263.26$. We also use in both the Hamiltonian and overlap, $pp\pi = -pp\sigma/2$ and $pd\pi = -pd\sigma/\sqrt{3}$.

Calculations of static bulk properties using these models are shown in table 2. The TB models are in as good agreement as could be expected from an approximate quantum mechanical theory. Although the discrepancies are noticeably worse than a typical fitted classical potential, we shall see later that the models for Nb are a go deal more reliable. It would also not be possible to find a classical potential that could describe the change in phase stability going from Mo to Re. Parameters for the Mo–Re bond are taken as the geometric mean of those of Mo–Mo and Re–Re. These are tested in the setting of a hypothetical MoRe alloy in the CsCl structure and the results in table 2 are compared with LDA calculations. The agreement is fair: at least the TB model correctly predicts the positive heat of formation of the compound.

It is important to note that the non-orthogonal spd model for Nb, in spite of the improved band structure, is in

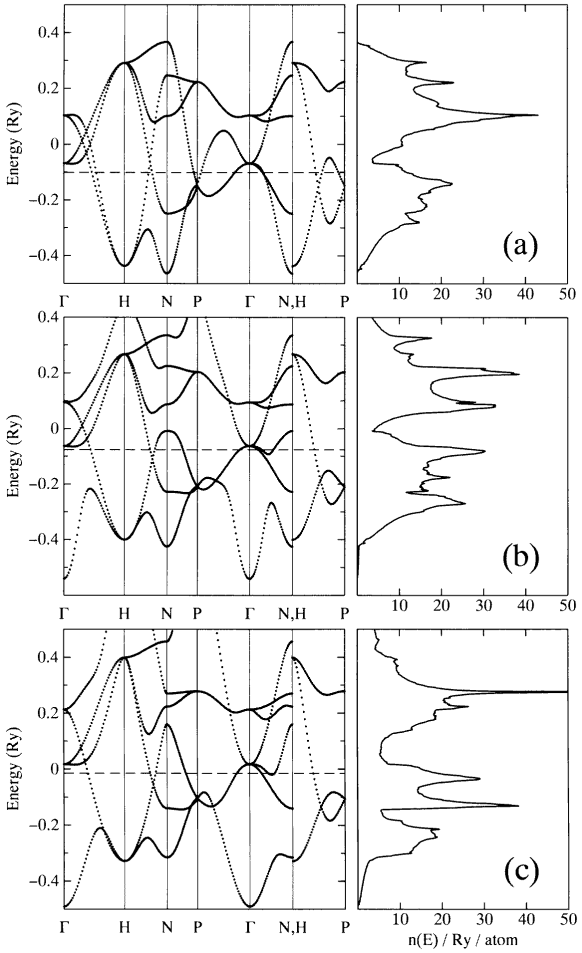

Figure 3. Energy bands and densities of states in Nb. (*a*) d-band TB model, (*b*) spd TB model, (*c*) local density approximation.

significantly worse agreement for the properties in the table than the simpler orthogonal d-band model. The cohesive energy is improved for reasons stated in connection with figure 1 (above)—the comparison is with a LDA result not corrected for the spin polarization of the free atom: this is the correct comparison to make in this case. Another important point to make here is that the inclusion of valence–valence overlap *does not* provide a positive sp-pressure sufficient to balance the attractive d-pressure as in figure 1. The spd model still employs a large pair potential albeit somewhat weaker than in the d-band model (compare parameters *b* and *p*). As mentioned earlier the valence–core overlap is the principal source of the positive pressure and this is missing in the TB model [17].

Energy–volume curves for close-packed and non-close-packed structures are shown in figures 4 and 5. These can be compared with those for the first-row transition metals in [18]. The reasonableness of the models is amply confirmed here. Again, a part from the cohesive energy, the spd model for Nb is less sensible than the simpler d-band model.

Table 2. Calculated equilibrium properties compared to experiment (parentheses) or local density approximation [brackets]. Values in {braces} are those involved in the TB fit, namely, the lattice constant a which is in Bohr. c/a is the hcp axial ratio; C' is $(c_{11} - c_{12})/2$ and K is the bulk modulus—these are given in GPa; H_f the heat of formation and E_B the cohesive energy are in mRy/atom; bcc–fcc and hcp–fcc (also in mRy/atom) are energy differences between close-packed phases.

		a	c/a	C'	c_{44}	K	E_B	H_f	bcc–fcc	hcp–fcc
Mo		{5.95}		112	126	299			−27	3.0
				(151)	(109)	(262)			[−34]	[2.6]
Re		{5.22}	1.610						28	−2.2
			(1.614)						[26]	[−5.9]
MoRe		5.89		91	143	340		+1.4		
		[5.89]		[89]	[217]	[299]		[+8.5]		
Nb	d	{6.22}		41	34	180			−17	3.4
Nb	spd	{6.22}		24	16	225	0.81		−17	4.6
				(56)	(30)	(172)	[0.79]		[−30]	[0.9]

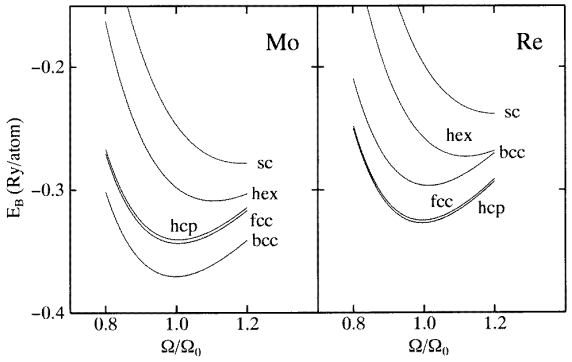

Figure 4. Cohesive energy versus atomic volume Ω, in the TB approximation. Ω_0 is the equilibrium volume.

1.4. Method of calculation

In either the DFT or the TB approach we use a similar method for the calculation of interface structure. A repeating unit cell or supercell is constructed, large enough so that any unphysical interaction between the repeated interfaces is prevented. This can be tested easily using the TB approximation since the band structures in either case will be similar and so if a supercell size is found to be sufficient in the TB case, then it can be assumed that it will also be so in the more expensive, computer intensive, DFT calculation. Further details on supercell construction are given in the following sections.

2. A grain boundary in Nb

Models for interatomic forces were given in section 1 without mentioning the importance of non-quantum mechanical (classical) prescriptions upon which the majority of atomistic simulation has been based in the past. The latter include pair potentials [19] and so-called pair functionals [20]. The subject of this section is a recent paper by Campbell *et al* [21] who demonstrated a serious error in the application of the pair functionals known as Finnis–Sinclair and embedded atom potentials to the structure of a grain boundary in Nb. The authors studied the (310)[001] symmetric tilt boundary in Nb;

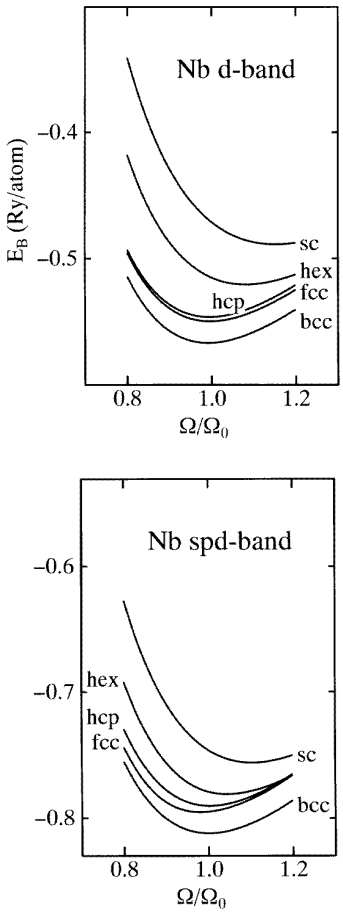

Figure 5. Energy–volume curves for Nb using the d-band and spd TB models.

firstly by atomistic simulation and secondly by high-resolution electron microscopy. The structure of the holosymmetric bicrystal is shown in figure 6 projected down the [001] tilt axis. Planes parallel to the paper are continuous across the interface (in other words, there is a colour reversing mirror plane m'). This is the structure that Campbell *et al* found to be the only minimum using a sophisticated many-atom expansion called MGPT (model generalized pseudopotential theory) constructed by

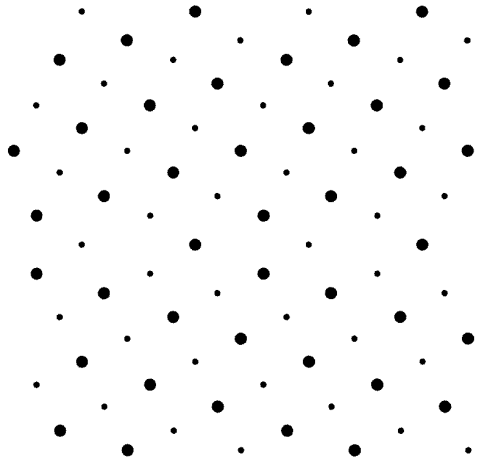

Figure 6. Relaxed global minimum structure of the (310)[001] symmetric tilt boundary in Nb. The projection is on the tilt axis [001], [310] points up the page and [1$\bar{3}$0] to the left. There are two planes of atoms in the repeat distance along the tilt axis separated by $a/2$: these are shown as large and small circles.

Moriarty [22]. However, using pair functionals they found other local minima, the two lowest energy ones having a translation of $a/2$ along the [001] tilt axis. The HREM clearly revealed that the grain boundary was not translated along the tilt axis, in other words the m' symmetry element was not destroyed by relaxation.

Figure 7 shows perspective representations of the untranslated and translated grain boundaries. Figure 7(a) shows a basic unit of the holosymmetric bicrystal, the two crystals coloured black and white with grey atoms shared by both grains. The basic structural unit is a capped triangular prism that can be seen as a consequence of the placement of two body-centred cubes with a common [001] edge but rotated about that edge by 36.9° (the $\Sigma = 5$ misorientation). The amount of expansion (translation normal to the boundary plane) is expected to be controlled by a competition between a local increase in volume inside the prism and the compression of the bond across the interface joining the black and white atoms as illustrated. Figure 7(b) shows a similar view of the translated grain boundary. The capped rectangular face on the prism has become a diamond shape, the compressed bond has lengthened and there are now two bonds per atom across the interface increasing the coordination of those atoms. This is done at the expense of large angular distortions of the two cubes above and below the grain boundary. One can see then, why a pair functional having no angular terms would favour the translated interface over the holosymmetric structure.

Our TB model, in agreement with MGPT and experiment, finds just one minimum, namely the holosymmetric untranslated structure. Calculations were done using a supercell of grain boundaries separated by ten layers of perfect crystal. Brillouin zone integration was by an improved tetrahedron method [23] using 400 $\boldsymbol{k}$-points in the whole zone. It was found that increasing the size

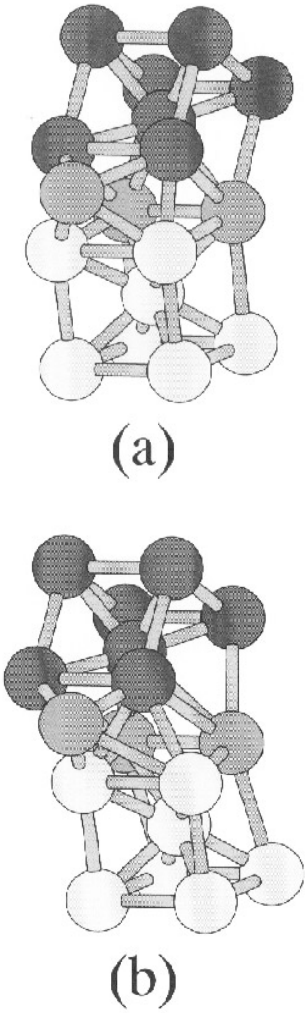

Figure 7. (a) A perspective view of the local atomic structure at the grain boundary illustrated in figure 6. A body-centred cube of the lower (white) crystal is joined along the [001] cube edge to a cube of the upper (black) crystal, but misorientated by 36.9°. Atoms in the interface are coloured grey. Note how three black, three white and three grey atoms make up a capped triangular prism, the structural unit of this grain boundary. The bond between the white and black atoms is compressed and a hole, like a vacancy, appears inside the prism. (b) The same structure in which the white crystal is translated with respect to the black by $a/2$ along the [001] tilt axis. Note that an extra bond appears across the boundary and that the bcc cubes are angularly distorted.

to twenty layers did not significantly affect any results. Instead of using flexible boundary conditions, the supercell was relaxed using molecular statics at constant volume at a number of different values of imposed expansion (or equivalently, supercell length). Charge self-consistency was not used in these calculations. Figure 8 shows a plot of the relaxed grain boundary energy as a function of the expansion, which is a measure of the increase in (310) interplanar spacing across the boundary relative to the bulk (310) spacing (i.e. an expansion of zero means no change in interplanar spacing going across the grain boundary).

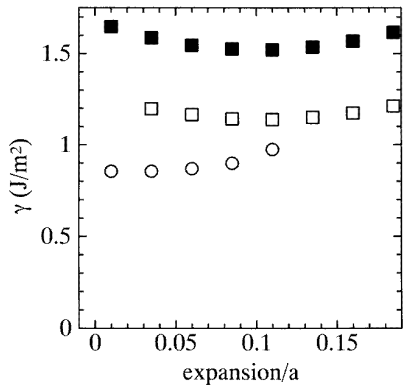

Figure 8. Grain boundary energy γ as a function of imposed expansion. The expansion is in units of the lattice constant and is expressed as the excess expansion across the grain boundary compared to the bulk (310) interplanar spacing. The black squares represent the relaxed energy from the d-band tight-binding model, the open squares from the spd model and the circles the energy in the local density approximation for the structures relaxed with the d-band model. Note that the TB approximation overestimates the expansion which the LDA predicts to be close to zero.

For each relaxed structure at a given expansion, we have then calculated the total energy, equation (1), and hence grain boundary energy in the local density approximation using the FP–LMTO method. These results shown in figure 8 are quite revealing. Firstly we get a quite accurate estimate of the absolute grain boundary energy; secondly we see that the LDA predicts a slightly smaller expansion than the TB approximation. In fact the compressed bond across grain boundary pointed out in figure 7 has a length of 2.67 Å in the TB model (compared to the equilibrium bond length of 2.85 Å); in the local density approximation this bond length is 2.62 Å. This close proximity of the atomic columns across the grain boundary has been noticed in a recent analysis of HREM images [24]. Note that both the LDA and TB results agree with this experimental finding, although the TB calculation underestimates the extent to which these columns are compressed.

Also shown in figure 8 is the grain boundary energy versus expansion calculated using the non-orthogonal spd model. The discrepancy between TB and LDA concerning the competition between compressing a bond and making an open space inside the prism is not improved, demonstrating again that the spd model does not improve the description of volume-dependent terms. The grain boundary energy is closer to the LDA result, but this may be fortuitous. We cannot conclude that the spd model is any improvement over the simpler and more pleasing d-band model.

3. A dissimilar metal interface in the Mo–Re system

The refractory metals are receiving a revival of engineering interest [25, 26] as they are regarded as promising components in nuclear motors and energy converters for the space programme. Re and Re–50% Mo are high-strength, ductile, weldable, refractory metals. Re–50% Mo also has a high neutron capture cross section. They are finding particular application in heat exchangers in a hydrogen environment and as coatings for rocket engine exhaust nozzles. It also happens that this system of metals lends itself to atomistic modelling. As discussed above, what seems like a reliable TB model can be made. An interface that is of interest to study can be constructed by joining the $(10\bar{1}0)$ prism face of the hcp Re to the (110) face of bcc Mo. This is illustrated in figure 9. The [0001] c-axis in Re is exactly the length of the $[1\bar{1}0]$ lattice vector in Mo so that the interface is lattice matched in that direction with a periodicity of the Re c-axis. In the direction in the interface at right angles to that, the [001] lattice vector of the Mo is parallel to the $[11\bar{2}0]$ a-axis of Re and the lengths of these two lattice vectors are in the ratio 8/7 so that in this direction the interface is also periodic but with a repeat distance of 7 Mo or 8 Re lattice spacings. This Mo/Re interface is therefore periodic in both directions but has a lattice mismatch in one direction only that might be expected to result in a single array of parallel misfit dislocations, if the misfit were to be localized. This interface is then a useful model for studying the core structure of misfit dislocations, the strength of lattice-mismatched interfaces, the effect of interdiffusion and even maybe the point defect–dislocation interaction. All this could probably be reliably done within the context of the TB model, backed up by some first principles calculations as in section 2.

The remainder of the paper will describe some calculations intended to be a start in this direction. Calculations are done in supercells and as above tetrahedron integration is used with 72 $\boldsymbol{k}$-points in the whole Brillouin zone. The size of the supercells is such that there are eight layers of Re atoms and five layers of Mo before the cell repeats itself along the y-direction (figure 9). We have done some tests using larger cells and are convinced that the electronic structure is converged at this supercell size.

The separation h between the crystals should, ideally, be relaxed along with the atom positions. Instead we have determined h for the unrelaxed cell and used that value as fixed. All relaxations subsequently are at constant volume. As mentioned at the end of section 1.2, we also perform the self-consistency procedure separately from the atomic relaxations. That is to say, we first relax the positions and then make the Hamiltonian self-consistent. We have found that after doing this, further relaxations are not significant. Finally, we calculate the total energy of the supercell using twice the number of $\boldsymbol{k}$-points.

3.1. Molecular statics and dynamics calculations

The interface shown in figure 9 can be relaxed with molecular statics, in which case the structure shown in figure 10 is found. There is a local minimum without any translation in the z-direction (figure 9) and the region close to the shaded atom can be identified as the core of a misfit dislocation.

However, when the structure is relaxed using molecular dynamics, then a global minimum is found having a

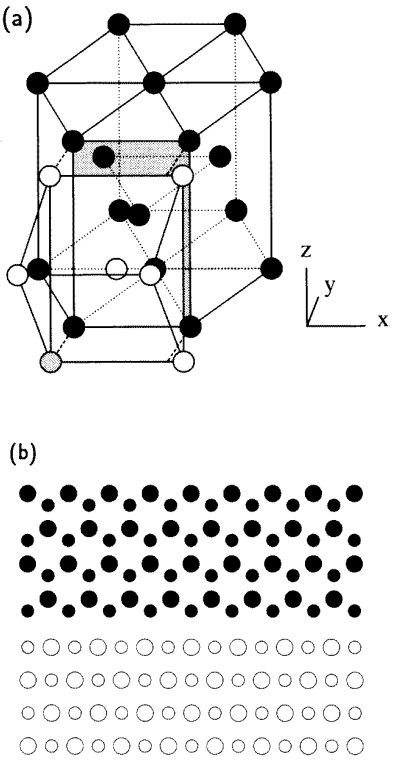

Figure 9. (*a*) Juxtaposition of the Re hcp and Mo bcc lattices. Planes parallel to the interface are shown shaded. The *z*-direction is parallel to $[1\bar{1}0]_{Mo}$ and $[0001]_{Re}$. In this direction the structure repeats itself every repeat of the hcp *c*-axis which is equal in length to $\sqrt{2}a_{Mo}$. The *x*-direction also lies in the interface and is parallel to the *a*-axes of Mo and Re which differ in length in the ratio 8/7; the interface is therefore mismatched in this direction but repeats every 7 Mo and every 8 Re lattice spacings *a*. The *y*-direction is normal to the interface and parallel to $[110]_{Mo}$ and $[10\bar{1}0]_{Re}$. The distance *h* between the two crystals is shown as a broken line. The total energy will be minimized with respect to *h*. (*b*) A projection of the Mo/Re interface down the *z*-axis of figure 9(*a*). Only two planes of atoms need be shown in this direction as the structure then repeats itself. These two planes are shown as large and small circles. The *x*-axis points to the right and the figure shows 7 Mo and 8 Re lattice spacings in this direction after which the structure repeats itself. The *y*-axis points upward. Note the disregistry in the interplanar spacing across the interface. The same Mo atom in both figures is lightly shaded to emphasize the relation between the two perspectives.

translation along the z-axis of half the periodicity in that direction. This is illustrated in figure 11.

In conclusion,. two local minima are found. In the global minimum, there is no obvious 'core' to the misfit dislocation and the disregistry is spread evenly across the interface. In the other (local) minimum, the disregistry is rather more localized and the dislocation core can be thought to be centred at the shaded atom in figure 9 which is a region of high energy with a Mo and a Re atom facing each other at rather a short distance across the interface.

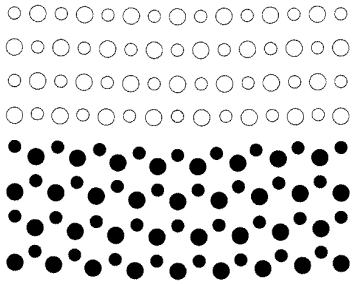

Figure 10. Structure of the relaxed, untranslated interface. The shaded atom corresponds to that in figure 9(*b*) and appears at the core of the misfit dislocation.

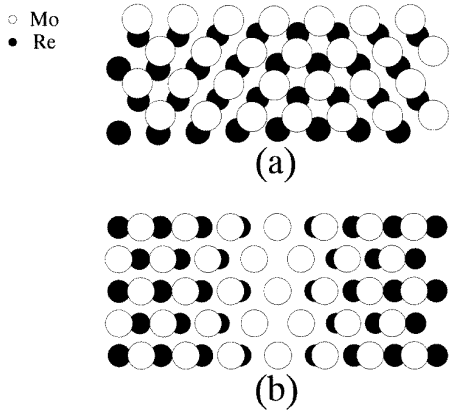

Figure 11. The interface viewed along the *y*-direction (i.e. face on) showing just the single Re and Mo layers on either side of the interface. (*a*) The translated structure, global minimum; (*b*) the local minimum found with molecular statics and showing greater localization of the misfit at a dislocation.

3.2. Calculation of the response to an applied shear strain

The relaxed structure of the local minimum was shown in figure 10. As expected, to the left and right parts of the interface, the disregistry between atomic planes across the interface has improved at the expense of the appearance of a dislocation core at the centre. In other words, the disregistry which is evenly distributed across the unrelaxed interface as well as the relaxed global minimum has become localized at the core of a misfit dislocation after atomic relaxation.

In a series of simulations in molecular statics, we apply successive shear strains to the atomic cell. It is clear from a study of figure 9 that if we displace the (upper) Re block with respect to the (lower) Mo block by a vector of length $b = a_{Mo} - a_{Re} = 1.38$ Å in the x-direction, then we would recover an identical atomic structure. This is the translational periodicity of the interface in the x-direction; it is also the length of the 'cell of non-identical displacements', (CNID) [27] or 'DSC' vector, as well as the magnitude of the Burgers vector b of the misfit dislocation. In this process, the dislocation will move through a distance a_{Mo}, the Mo lattice constant, achieving a plastic strain of the interface. The energy barrier involved in this process is

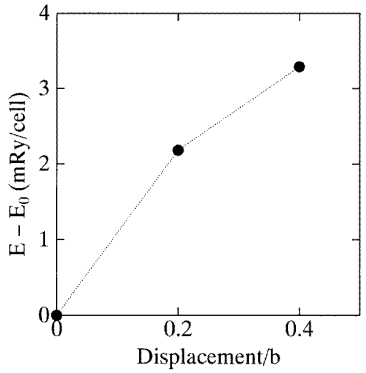

Figure 12. Energy E of the interface relative to the energy of the undisplaced structure in figure 11(a), E_0. The displacement is in units of the translational period b of the interface.

then calculated. Unlike a lattice dislocation, the interfacial dislocation moves a distance $a_{Mo} \gg b$ to achieve an amount of slip equal to b.

Beginning with the relaxed structure shown in figure 11(a) we apply a strain of $0.2b$ by adjusting the boundary conditions of the supercell (see [1], p 169 for details of how this is done). We re-relax the atomic positions, make the Hamiltonian self-consistent and obtain the total energy of the cell for this displacement. Using the new, sheared structure we apply another strain of $0.2b$ and repeat the procedure. We continue to shear the cell by increments, relaxing the positions and the Hamiltonian at each step. We obtain a plot of the energy of the cell versus shear, as shown in figure 12. We only show displacements up to $0.4b$; for larger values we have encountered problems in determining the minimum from a number of metastable states. By symmetry, however, we know that the curve must be symmetrical about $b/2$.

We may loosely think of the calculation as a way of determining the Peierls energy for the dislocation motion. As the dislocation moves from one Peierls valley to the next (a distance a_{Mo} away) the energy barrier ΔE is of the order of 3 mRy (0.04 eV). The displacement is b so that the stress is, very approximately,

$$\tau \approx \frac{2\Delta E}{b \cdot A_{cell}}$$

where A_{cell} is the area of the interface in the unit cell. This is about 0.4 GPa which is more than ten times smaller than the theoretical strength which must be of the order of 10–20 GPa. However, the interface is not significantly 'weakened' by the misfit dislocation. An almost identical result is obtained if the structure in figure 11(b) is used as a starting point. It seems that the ideal strength is not sensitive to whether the misfit dislocation is localized or spread out.

The interpretation of this as a Peierls stress is not really admissible. What has been calculated here is a small part of the 'relaxed gamma surface' defined by Vitek [28]. This does have an interpretation in terms of the strength of the interface [29, 30] but not directly as a Peierls stress. This would only be true if an additional, lattice dislocation were introduced into the problem. As pointed out by Sutton [31], as the CNID vector b tends to zero, so the fully relaxed gamma surface will become flat. This does not mean that an irrational boundary has zero resistance to shear, but that the relaxation processes involve collective movements of atoms that cannot occur on the timescale of the applied strain rate. The calculations in figure 12, therefore, are useful only in the sense of an attempt to find the relaxed gamma surface, and to see how the theoretical strength of the interface differs from the bulk crystal. To determine the dynamics of dislocation motion is a more complex problem.

4. Conclusions

In this paper, we have taken up a *Leitmotif* of this conference, as explained by Rühle in these proceedings [32] which is the study of interfaces using *reliable* prescriptions for interatomic forces—specifically concentrating on the translation state of the boundary. This is one of the principal degrees of freedom of an interface measured by HREM.

An approach which seems promising, and which is adopted here, is to use a combination of quantum mechanical schemes—one first principles and wholly reliable (but expensive) and the other empirical, but embodying sufficient rigour to have predictive power as well. The DFT calculations are used mainly to provide data with which to fit the empirical Hamiltonian, but also to make checks on the total energies of structures relaxed with the tight-binding scheme.

We have seen that quite adequate TB models for Mo, Re and Nb can be made; and in the latter case the simple d-band model is not improved by the inclusion of the sp-bands and non-orthogonality. Calculations of the atomic structure of the (310) symmetrical tilt boundary are completely consistent with experiment, and a check using density functional theory shows that the energy and translation state are in good agreement with the approximate TB model.

The TB model for Mo and Re is then used to make some calculations of the atomic structure and relaxed gamma surface of a long period Mo–Re interface. This work is only introductory at this stage, but it illustrates what can be done in heterogeneous systems and serves to exemplify some of the principles involved.

Acknowledgments

I have enjoyed valuable conversations with Peter Gumbsch, John Klepeis and Adrian Sutton. Michael Methfessel and Mark van Schilfgaarde kindly provided their FP-LMTO computer program. This work was supported in part by the US-ONR under contract N0001492C0006 and by the EPSRC under grants GR/K03968 and GR/H58278-C80.

References

[1] Pettifor D G and Cottrell A H (ed) 1992 *Electron Theory in Alloy Design* (London: Institute of Materials)
[2] von Barth U and Hedin L 1972 *J. Phys. C: Solid State Phys.* **5** 2064
[3] Methfessel M 1988 *Phys. Rev.* B **38** 1537
[4] Foulkes W M C and Haydock R 1989 *Phys. Rev.* B **39** 12520
[5] Sutton A P, Finnis M W, Pettifor D G and Ohta Y 1988 *J. Phys. C: Solid State Phys.* **21** 35
[6] Finnis M W 1992 *Acta Metall. Mater.* **40** Suppl. S25
[7] Harrison W A 1985 *Phys. Rev.* B **31** 21
[8] Robbins M O and Falicov L M 1984 *Phys. Rev.* B **29** 1333
[9] Chadi D J 1984 *Phys. Rev.* B **19** 2074; 1978 *Phys. Rev.* B **41** 1062
[10] Kohyama M, Yamamoto R, Ebata Y and Kinoshita B 1988 *J. Phys. C: Solid State Phys.* **21** 3205
[11] Pettifor D G 1977 *J. Phys. F: Met. Phys.* **7** 613
[12] Gellat C D Jr, Ehrenreich H and Watson R E 1977 *Phys. Rev.* B **15** 1613
[13] Andersen O K, Jepsen O and Glötzel D 1985 *Highlights of Condensed Matter Theory* ed F Bassani *et al* (Amsterdam: North-Holland) p 59
[14] Spanjaard D and Desjonqères M C 1984 *Phys. Rev.* B **30** 4822
[15] Gunnarsson O, Andersen O K, Jepsen O and Zaanen J 1982 *Core-level Spectroscopy in Condensed Systems, Springer Series in Solid-State Sciences* vol 81, ed J Kanamori and A Kotani (Heidelberg: Springer) p 82
[16] Skriver H L 1985 *Phys. Rev.* B **31** 1909
[17] Callaway J 1974 *Quantum Theory of Solids* (New York: Academic)
[18] Paxton A T, Methfessel M and Polatoglou H M 1990 *Phys. Rev.* B **41** 8127
[19] Vitek V 1976 *Crystal Latt. Def.* **5** 1
[20] Carlsson A E 1990 *Solid State Phys.* **43** 1
[21] Campbell G H, Foiles S M, Gumbsch P, Rühle M and King W E 1993 *Phys. Rev. Lett.* **70** 449
[22] Moriarty J A 1985 *Phys. Rev. Lett.* **55** 1502; 1990 *Phys. Rev.* B **42** 1609; 1990 *Many-Atom Interactions in Solids Springer Proc. Physics* vol 48, ed R M Nieminen *et al* (Berlin: Springer) p 158
[23] Blöchl P E, Jepsen O and Andersen O K 1994 *Phys. Rev.* B **49** 16 223
[24] King W E and Cambell G H 1995 Lawrence Livermore National Laboratory, private communication
[25] Titran R H 1992 *Adv. Mater. Proc.* **142** 34
[26] Bryskin B D 1992 *Adv. Mater. Proc.* **142** 22
Shields J A Jr 1992 *Adv. Mater. Proc.* **142** 28
[27] Vitek V, Sutton A P, Smith D A and Pond R C 1980 *Grain Boundary Structure and Kinetics* ed R W Balluffi (Ohio: American Society for Metals) p 115
Sutton A P 1984 *Int. Met. Rev.* **29** 377
[28] Vitek V 1968 *Phil. Mag.* **18** 773
[29] Paxton A T, Gumbsch P and Methfessel M 1991 *Phil. Mag.* A **63** 267
[30] Anderson P M and Rice J R 1986 *Scripta Metall.* **20** 1467
Rice J R 1987 *NATO Advanced Workshop on Chemistry and Physics of Fracture* ed R M Latanision and R H Jones (Dordrecht: Martinus Nijhoff) p 22; 1992 *J. Mech. Phys. Solids* **40** 239
[31] Sutton A P 1989 *Phase Trans.* **16/17** 563; 1992 *Prog. Mater. Sci.* **36** 167
[32] Yang J C, Schumann E, Müllejans H and Rühle M 1996 *J. Phys. D: Appl. Phys.* **29** 1716